JACS
JOURNAL OF THE AMERICAN CHEMICAL SOCIETY
Article
pubs.acs.org/JACS

A Solution-Phase Bifunctional Catalyst for Lithium–Oxygen Batteries

Dan Sun,[†] Yue Shen,*[,†] Wang Zhang,[†] Ling Yu,[†] Ziqi Yi,[†] Wei Yin,[†] Duo Wang,[†] Yunhui Huang,*[,†] Jie Wang,[§] Deli Wang,[§] and John B. Goodenough[‡]

[†]State Key Laboratory of Material Processing and Die & Mould Technology, School of Materials Science and Engineering, Huazhong University of Science and Technology, Wuhan, Hubei 430074, China

[§]School of Chemistry and Chemical Engineering, Key Laboratory of Large-Format Battery Materials and System, Ministry of Education, Huazhong University of Science and Technology, Wuhan, Hubei 430074, China

[‡]Texas Materials Institute, The University of Texas at Austin, ETC 9.102, 1 University Station, C2200, Austin, Texas 78712, United States

Supporting Information

ABSTRACT: A lithium–oxygen battery would deliver the highest energy density of a rechargeable battery, but the multiphase electrochemical reaction on the air cathode has difficulty proceeding when operated with only solid catalysts. We report here the organic-electrolyte-dissolved iron phthalocyanine (FePc) as a shuttle of $(O_2)^-$ species and electrons between the surface of the electronic conductor and the insulator Li_2O_2 product of discharge. The Li_2O_2 is observed to grow and decompose without direct contact with carbon, which greatly enhances the electrochemical performance. Our results signal that the use of molecular shuttles that are catalytically active may prove to be enablers of a practical lithium–air rechargeable battery.

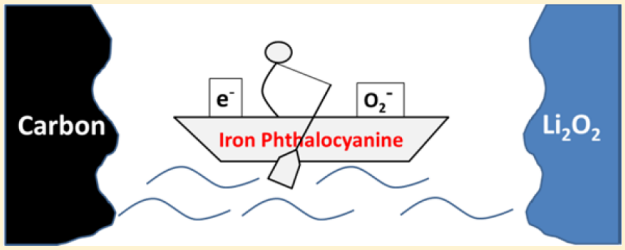

INTRODUCTION

The lithium–oxygen battery has received worldwide attention because it promises the theoretical reversible high-capacity limit for a rechargeable battery.[1−4] The cathode of a lithium–oxygen cell requires a catalyst that is active for both the oxygen-reduction and oxygen-evolution reactions (ORR and OER). Many solid cathode catalysts have been developed in lithium–oxygen batteries,[5,6] such as noble metals,[7,8] metal oxides,[7,9−14] Fe–N/C complexes,[1,15−17] carbon nanotubes/nanofibers,[18−21] graphene nanosheets,[22−25] perovskites,[26,27] pyrochlore,[28] et al. However, there are still some fundamental problems remaining for solid catalysts.[29] For example, since the discharge product Li_2O_2 is also in solid state, it will accumulate at the catalyst surface and hence block the electrode reactions during the discharge process. Meanwhile, during the charging process, it is also difficult to make good contact between the solid catalyst and Li_2O_2.[30,31] Theoretically, the above problems will be alleviated if a solution-phase catalyst is used to catalyze the formation and decomposition of the solid Li_2O_2. A very recent work showed that incorporation of a redox mediator greatly improved the charging performance of the Li–O_2 battery.[32−34] But so far, the solution-phase catalysis is still an unexplored field.

In this work, we report organic-electrolyte-dissolved iron phthalocyanine (FePc) as the catalyst for both discharge and charge processes in lithium–oxygen batteries. It acts not only as a redox mediator, but also as a molecular shuttle of $(O_2)^-$ species between the surface of the electronic conductor and the insulator Li_2O_2 product of discharge.

RESULTS

Electrochemical Properties of FePc. Although it is well-known that molecular FePc is active for the ORR,[35−38] FePc is not soluble in aqueous electrolytes and has a poor electronic conductivity; therefore, it is not applicable in conventional proton-exchange membrane (PEM) fuel cells. However, FePc can be dissolved in some organic electrolytes such as dimethyl sulfoxide (DMSO)[30,39] and tetraethylene glycol dimethyl ether (TEGDME),[40,41] as seen in Figure 1a; it can be used in a lithium–air cell. If we induce some O_2 or LiOOLi powder to the diluted FePc solution, we will observe a red shift of the

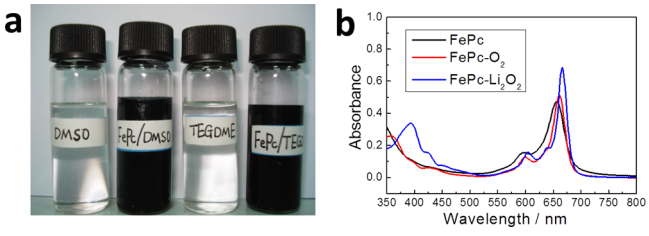

Figure 1. Electrochemical properties of FePc. (a) Photo of the DMSO and TEGDME electrolytes with or without 0.002 mol L^{-1} FePc. (b) UV–vis absorption spectra of the FePc, FePc–O_2 and FePc-LiOOLi (1.5×10^{-5} mol L^{-1}).

Received: February 22, 2014
Published: May 14, 2014

 © 2014 American Chemical Society

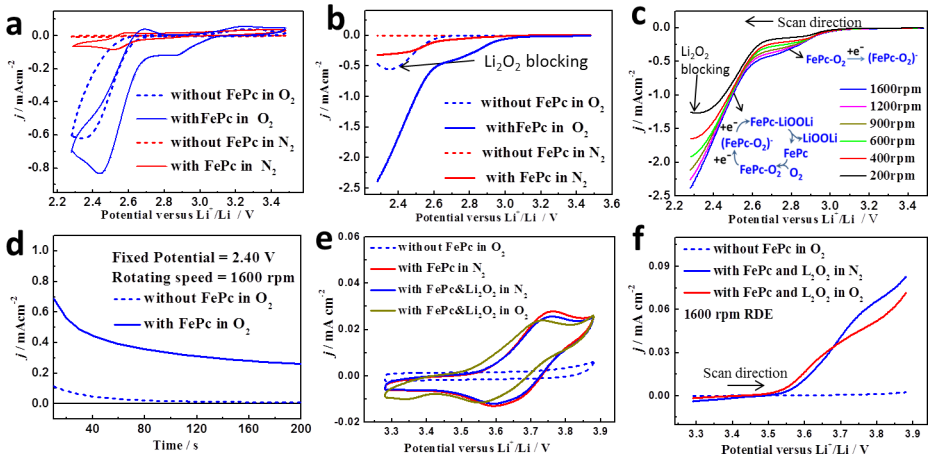

Figure 2. (a,b) ORR potential range CV (a) and fixed speed RDE (b) measurement of the DMSO-LiTFSI electrolytes with/without FePc in inert/oxygen atmosphere. (c) Changing the speed of the RDE measurement of the DMSO−LiTFSI electrolyte with FePc in oxygen atmosphere. (d) Current decrease with different electrolytes in fixed potential RDE measurement. (e,f) OER potential range CV (e) and RDE (f) measurement of the DMSO−LiTFSI electrolytes with/without FePc−Li_2O_2 powder. CV potential scan rate = 50 mV s^{-1}, RDE potential scan rate = 5 mV s^{-1}.

UV−vis absorption peak, indicating that dissolved FePc is easy to coordinate with O_2 and LiOOLi (Figure 1b).[42]

In the absence of oxygen, the cyclic voltammetry of FePc (Figure 2a and e) reveals two redox reactions, a complex Fe^{III}/Fe^{II} reaction near 3.65 V versus Li^+/Li^0 and an Fe^{II}/Fe^{I} near 2.5 V.[37,43] In the presence of oxygen, the FePc coordinates with oxygen, and the Fe^{II}/Fe^{I} reaction shifts to 2.86 V (Figure 2a). The $(FePc-O_2)^0/(FePc-O_2)^-$ transition can be regarded as the result of both Fe^{II}/Fe^{I} reaction and oxygen-reduction reaction. $(FePc\text{-}O_2)^-$ has several resonance structures because of the delocalization of the negative charge. If the negative charge is on the Fe atom, it can be viewed as Fe(I); if the negative charge is on the O_2 ligand, it can be viewed as a reduced oxygen. Similar to some natural enzymes with transition metal and macrocyclic ligand,[44] the $(FePc-O_2)^-$ can be further reduced into $(FePc-O_2)^{2-}$ and combine with two lithium ions to form FePc−LiOOLi. The LiOOLi may dissociate from the FePc and nucleate in the electrolyte, and then the FePc can catalyze the reduction of another oxygen molecule.

The ORR activity testing was performed on a rotating disk electrode (RDE). As shown in Figure 2b, the onset potential shifts significantly positive with the existence of FePc in the solution, indicative of excellent electrocatalytic activity of FePc for ORR. With FePc, the ORR polarization curve shows two stages (Figure 2c), agreeing with the "$(FePc-O_2) \rightarrow (FePc-O_2)^- \rightarrow$(FePc−LiOOLi)" two-step mechanism. By using the Levich equation, the number of electrons transferred in the first step reaction is estimated to $1.14 \approx 1$ if we assume that the diffusion coefficients of FePc and FePc−O_2 in DMSO are the same (the calculation is described in detail in the Supporting Information [SI]). Another interesting phenomenon is the "LiOOLi blocking effect" in the low potential region. In the system without FePc, at a rotation rate of 1600 rpm, the current density decreased when the potential was scanned below 2.33 V. This unusual phenomenon is because the reaction product, solid LiOOLi, accumulated on the electrode surface and deactivated the electrode. To confirm this point, the current was measured at fixed potential 2.40 V (Figure 2d). Without FePc, the current decreased to near zero because of LiOOLi blocking. On the contrary, with FePc, the current was much larger because the FePc−LiOOLi compound is soluble; the LiOOLi may nucleate away from the carbon surface. The LiOOLi blocking effect is also confirmed in Figures S1 and S2 in the SI.

The FePc coordination complex can be oxidized and reduced around 3.65 V (Figure 2e). It may serve as a shuttle to transfer the charge from the electrode surface to the lithium peroxide in the OER process. An RDE experiment with additional lithium peroxide powder demonstrates the contribution of FePc to the oxidation current (Figure 2f). Without FePc, although Li_2O_2 particles were suspended in the electrolyte, there was no current because of the poor contact between the electrode and Li_2O_2. This is a common problem for OER in lithium−oxygen batteries. With FePc, the oxidation current increased significantly. The oxidation current in the OER potential range is not sensitive to the oxygen. The detailed catalytic mechanism of FePc for OER will be discussed in a later section.

Catalytic Activity of FePc in Lithium−Oxygen Batteries. We tested the catalytic activity of FePc dissolved in oxygen-containing TEGDME or DMSO electrolyte with a cathode composed of carbon fibers (CFs). Initially, no solid catalyst existed on the CFs. For comparison, we tested the catalytic activity at a CF cathode with a solid Fe−N/C catalyst but no FePc dissolved in the electrolyte. The solid Fe−N/C is a well-known solid catalyst for the ORR.[1,15−17,36] Finally, we tested a cathode with Fe−N/C attached onto the CFs and FePc in the electrolyte.

The CFs were obtained by carbonization of an electrospun mixture of polyacrylonitrile (PAN) and polymethylmethacrylate (PMMA) fibers.[45] (Figure S3 in the SI) The composition of the CFs can be easily modified by adding precursors into the electrospinning solution, which allows us to fabricate morphologically similar CFs with and without a solid state catalyst. We incorporated the solid Fe−N/C catalyst into the CFs by adding FePc into the polymer solution before electrospinning and carbonization. Energy dispersive X-ray spectroscopy (EDX, Figure S4 in the SI) and X-ray photoelectron spectroscopy (XPS, Figure S5 in the SI) results indicate the composition of our Fe−N/C CFs composite is comparable to that of the Fe−N/C catalyst previously reported for a lithium−air battery.[17]

Figure 3 compares the half-cell discharge/charge voltage profiles for the CFs with different catalysts and different

dx.doi.org/10.1021/ja501877e | J. Am. Chem. Soc. 2014, 136, 8941−8946

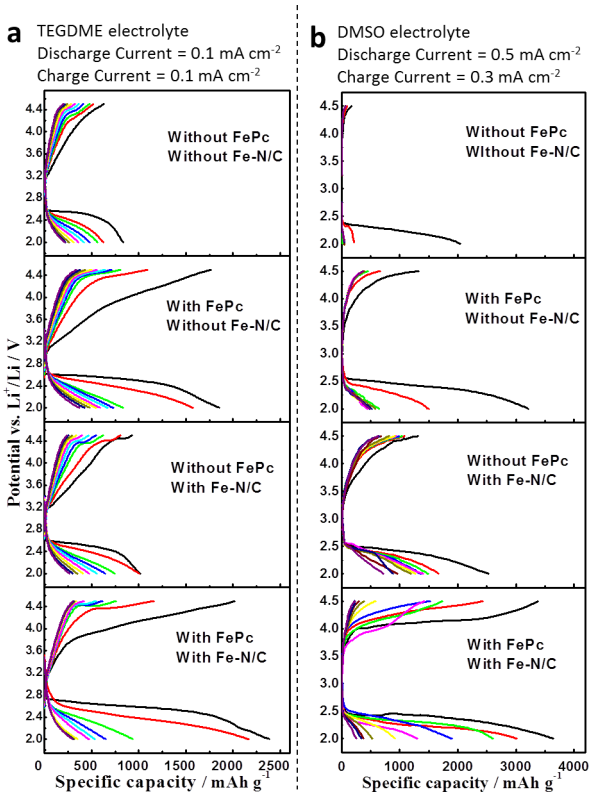

Figure 3. (a,b) The effects of different catalysts on the discharge–charge performance with TEGDME (a)- or DMSO (b)-based electrolytes.

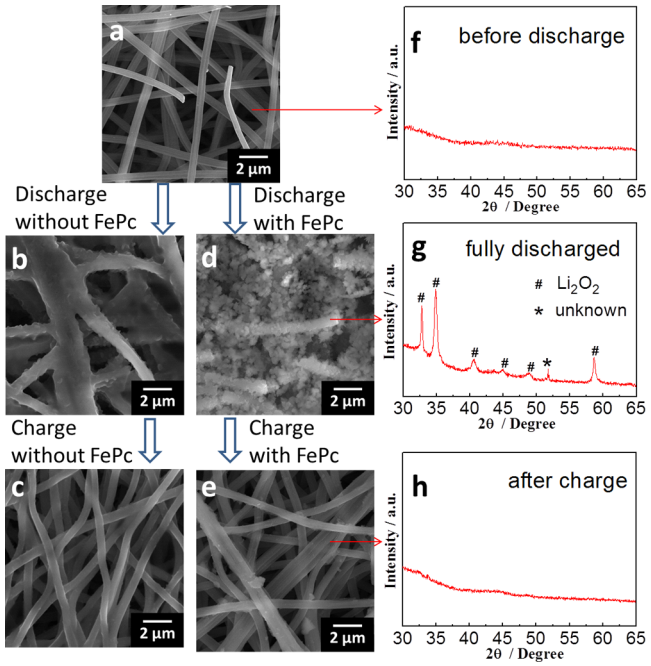

Figure 4. (a–e) SEM images of the CF cathodes (with Fe–N/C) before discharge (a), after discharge (b,d) and after charge (c,e) with FePc catalyst (d,e), and without FePc catalyst (b,c). (f–h) XRD pattern of the CF cathode before discharge (f), after discharge (g), and after charge (h) with FePc dissolved in the TEGDME electrolyte.

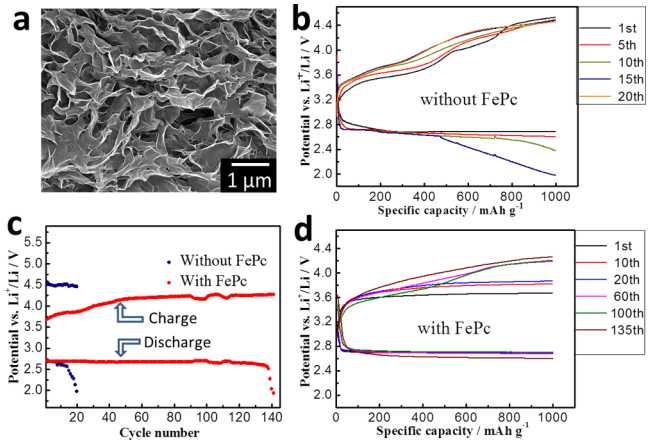

Figure 5. (a) SEM image of the graphene sponge. (b) Cycle performance of the battery without FePc. (c) Cycle performance of the battery with FePc. (d) The discharge and charge end potentials at different cycles.

electrolyte solvents. We noticed that dissolved FePc showed obvious catalytic activity toward both ORR and OER processes. Much improved discharge capacity and lower charge potential were obtained in both TEGDME and DMSO electrolytes by adding FePc. Because the viscosity of the DMSO was lower than the TEGDME, the DMSO-based batteries were able to tolerate higher discharge and charge current density. Furthermore, the dissolved FePc and solid Fe–N/C catalysts are compatible and work synergistically. The batteries' performance was best when both of the FePc and the Fe–N/C were used.

Interestingly, the FePc changed the morphology of the Li_2O_2 product of the discharge (Figure 4). Without the FePc, the Li_2O_2 formed during discharge covers the surface of the CFs (Figure 4b) whereas with the FePc in solution, Li_2O_2 deposited not only on the CF surface, but also on the Li_2O_2 itself until the Li_2O_2 almost fills the space between the CFs (Figure 4d). This morphology change demonstrates that with FePc in solution, the deposited Li_2O_2 blocks neither the catalytically active surface nor the catalytic ORR of the dissolved FePc if it is aggregated into particles. Both SEM and XRD results show that the Li_2O_2 was decomposed after the charge, which agrees with the capacity increase and reversibility improvement in Figure 3.

The replacement of the CFs with a graphene sponge can improve the cathode performance, especially the cyclability, as shown in Figure 5. The graphene sponge is a porous, ultralight, flexible, conductive material consisting of graphene nanosheets[46](Figure 5a). The average space between the graphene nanosheets is about 200 nm, which is much smaller than the ~2 μm space between the CFs. The average diffusion distance for the dissolved catalyst is, thereby, shortened considerably.

The cells assembled were tested with a homemade device to suppress the DMSO evaporation (Figure S6 in the SI). The discharge and charge capacities were limited to 1000 mA h g^{-1}; the discharge current was 0.5 mA cm^{-2}, the charge current was 0.3 mA cm^{-2}. Without the FePc, the cell failed at the 21st cycle; with the aid of FePc, the discharge curves exhibited a flat plateau at 2.69 V fading only to 2.67 V after 130 cycles. The charge end potential increased steadily over the first 50 cycles and leveled off at about 4.22 V from the 50th to the 130th cycle. The decomposition of electrolyte at high voltage is a major reason for the Li–O_2 battery performance decay. It is very difficult to totally eliminate these side reactions. However,

dx.doi.org/10.1021/ja501877e | J. Am. Chem. Soc. 2014, 136, 8941–8946

since the FePc is effective for lowering the charging potential, it should be available to depress the electrolyte decomposition and improve the cyclability.

DISCUSSION

The catalysis mechanism of the FePc is proposed as follows: As illustrated in Scheme 1a, FePc is a 2D molecule containing low-

Scheme 1. Possible Catalyzed Reaction Routes

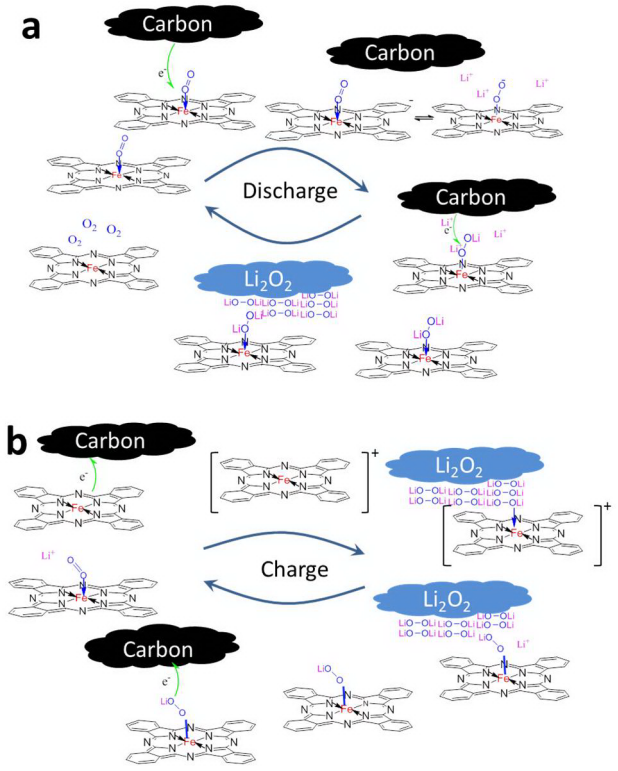

spin Fe^{II} coordinated by four square-coplanar N atoms; the nonbonding $(3z^2 - r^2)^2$ and $(yz \pm izx)^4$ orbitals are not filled. The nonbonding O-2p orbitals of an O_2 molecule are attracted to the positive core of the exposed Fe^{II} ion. According to Figure 1, we propose a "$(FePc-O_2) \rightarrow (FePc-O_2)^- \rightarrow$(FePc–LiOOLi)" two-step transformation mechanism. The (FePc–LiOOLi) would diffuse to a nucleated Li_2O_2 site, and then the LiOOLi part would separate from the FePc and incorporate into the crystal lattice of the Li_2O_2. In this process, the FePc–O_2 molecule serves as a shuttle of electrons from the carbon where it forms (FePc–LiOOLi) to a nucleated solid Li_2O_2 site where the Li_2O_2 grows. Such a process is consistent with the RDE data (Figure 2) and the SEM observation (Figure 4).

To apply this model to the reverse reaction on charge, we refer to Figure 2e. The reduction potential of oxidized FePc (3.55 V) is higher than the oxidation potential of LiOOLi (3.25 V), indicating that the Fe^{III} of $(FePc)^+$ can oxidize the $(O_2)^{2-}$ molecule of Li_2O_2 to reform $(FePc-O_2)^-$. The $(FePc-O_2)^-$ can diffuse back through the electrolyte to the carbon surface to be further oxidized into FePc and O_2. It is the energy of the Fe^{III}/Fe^{II} couple in the FePc molecule that allows oxidation of the Li_2O_2, and it is the ability of the solution-based $FePc(O_2)^-$ molecule to shuttle from the Li_2O_2 particles to the carbon surface near enough for electron transfer that makes possible the OER (Scheme 1b). This OER mechanism was also proposed in a previous patent.[34]

There are many differences between the solution-phase and solid-phase catalysts used in lithium–oxygen batteries, as listed in Table 1. In the ORR, the solution-phase catalyst transports

Table 1. Comparison of the Solution-Phase Catalyst and Solid-Phase Catalyst in Lithium–Air Batteries

catalyst type	solution phase	solid phase
catalyst–reactant contact	good	not good
reactions without carbon contact	yes	no
electronic conductivity	poor	good
molecular shuttle effect	yes	no
oxygen carrier	yes	no
influence to the anode	yes	no

the insulating Li_2O_2 product away from the carbon surface to prevent it from blocking the electron transfer needed to reduce the O_2. In the OER, the reactive sites of the solution-phase catalyst can be anywhere at the Li_2O_2 surface because of its diffusion. The contact between the solution-phase catalyst and the solid Li_2O_2 reactant is much better than that between the Li_2O_2 and a solid catalyst. But the electronic conductivity of the solution-phase catalysts is not as good as the solid-phase catalysts. So the solid-phase catalysts still have their own advantages on catalyzing reactions on its surface. Other than direct carbon–catalyst–reactant electron transfer, solution-phase catalysis involves some molecular shuttling through the electrolyte.[32,47] Thus, the diffusion rate and the average diffusion distance of the catalyst–reactant complexes may influence the total catalysis efficiency. Electrolytes with lower viscosity and cathode materials with smaller pore size are more favorable. It should also be noticed that the FePc is an oxygen carrier and enhances the solubility of oxygen. This is very good for both solution-phase and solid-phase catalysis.

As the FePc is dissolved in the electrolyte, it is possible to diffuse to the anode and cause some unfavorable side reactions. In organic-electrolyte lithium–air batteries, the solid electrolyte interphase (SEI) layer is an effective shield to prevent the oxygen–lithium direct contact[39,48] and slow down the anode direct oxidation rate to a tolerable level. In our case, the molecule size of FePc–oxygen is larger that of free oxygen, so it is more likely to be separated by the SEI. We disassembled two batteries with and without FePc after 10 cycles to see the stability of the lithium anode (Figure 6). The red circles in the figure indicate the area covered by the air cathode. The whole lithium anode was covered by the electrolyte wetted separator. The area out of the red circles was still shining, showing that the lithium anode is stable when steadily exposed in FePc-

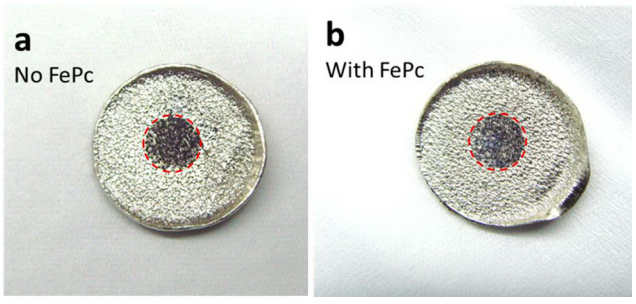

Figure 6. Photograph of the lithium anodes taken out of the coin cells after 10 cycles at 1000 mAh g^{-1}.

dx.doi.org/10.1021/ja501877e | J. Am. Chem. Soc. 2014, 136, 8941–8946

containing electrolyte and pure oxygen atmosphere. The area inside the red circles became dark for both FePc-containing and FePc-absent samples, which is because the SEI was damaged in the cycling process and the lithium dendrites might form and be oxidized. Some FePc may react or chemically adsorb on the anode surface. The analysis based on ICP-AES (inductively coupled plasma-atomic emission spectrometer) shows that the amount of Fe element on the anode after 10 cycles was about 1.7×10^{-9} mol, which was 11% of the original FePc total amount in the electrolyte. This effect may cause some FePc concentration decrease in the electrolyte and suppress the catalytic efficiency, but it should not be very serious. The overall lifetimes of FePc-containing batteries were much longer than those of the FePc-absent batteries. Which means that the influence of the FePc on the anode is tolerable.[49] To better solve this anode problem, we will need a more stable SEI layer or a thin oxide/polymer Li^+-electrolyte separator[50] that blocks dendrites from a lithium anode and migration of FePc from the cathode to the anode.

CONCLUSION

The FePc-based solution-phase catalyst has been proven to be effective in the discharge/charge process and to enable a rechargeable lithium−oxygen battery of large capacity. The Fe−oxygen coordination and the electron dislocation in the big conjugated structure lowers the energy of the high-energy intermediates in the ORR and OER. The dissolved FePc can act as a molecular shuttle of $(O_2)^-$ species and electrons between the surface of electronically conducting carbon and product Li_2O_2 particles. As a consequence, the Li_2O_2 is observed to grow and decompose without direct contact with carbon. We show that the synergy of the solid catalyst and the solution-phase shuttle catalyst is critical for achieving a high-capacity reversible lithium−oxygen battery.

EXPERIMENTAL SECTION

Preparation of the Electrolytes. The solvents, TEGDME and DMSO, were purchased from Sigma-Aldrich; both were further dried over freshly activated molecular sieves (type 4 Å) for 24 h. Lithium bis(trifluoromethane sulfonimide) (LiTFSI) was used as the lithium salt and was dried for 24 h in a vacuum chamber (pressure $<10^{-4}$ Pa) connected to the glovebox filled with Ar. The FePc (from Sigma-Aldrich) was also vacuum-dried. The electrolytes were prepared by mixing the solvent, LiTFSI, and FePc in the Ar glovebox. The concentration of the LiTFSI and FePc were controlled at 0.1 mol L^{-1} and 0.002 mol L^{-1}, respectively.

Cyclic Voltammetry (CV) and Rotating Disk Electrode (RDE) Measurement. The CV and RDE tests were performed on an electrochemical workstation (CHI760E, CH Instruments, Shanghai, China) with a rotating disk electrode system (Pine Research Instrumentation, U.S.A.). A glassy carbon disk electrode with 5 mm diameter was used as the working electrode. A piece of stainless steel mesh loaded with half-charged $LiFePO_4$ was used as the counter electrode. A standard calomel electrode (SCE) with a double bridge was used as the reference electrode. The electrolyte, composed of 0.1 mol l^{-1} LiTFSI and 0.002 mol l^{-1} FePc in DMSO solution, was prepared in the argon-filled glovebox. Nitrogen was induced into the electrolyte for 30 min to ensure the data measured in inert atmosphere. Then, pure oxygen was purged into the electrolyte for 10 min to study the ORR. Solid lithium peroxide powder was added to the electrolytic cell while stirring before use for the OER study.

Synthesis of the Carbon Fibers (CFs). One gram of PAN (M_w = 150,000 g mol^{-1}, Aldrich Co.) and 0.5 g PMMA (M_w = 99,100 g mol^{-1}) were dissolved in 10 mL dimethylformamide (DMF) under magnetic stirring at 60 °C for at least 24 h to obtain a homogeneous solution. Then the solution was transferred into a syringe with a 22 blunt needle. Electrospinning was carried out at 15 kV with a pump rate of 5 μL min^{-1}. The as-obtained electrospinning PAN/PMMA nanofibers were stabilized in air for 6 h at 280 °C, then were carbonized in N_2 at 650 °C for 3 h. After being cooled to room temperature the CFs were obtained. CFs with Fe−N/C were prepared according to the same procedures, but with the addition of 0.1 g FePc (M_w = 568.37 g mol^{-1}, Aldrich Co.) into the polymer solution before electrospinning.

Synthesis of the Graphene Sponge. Graphite flakes with average size of 500 μm were used to synthesize graphene oxide (GO) according to the previously reported process.[51] The scheme of the fabrication of the sponge with uniform thickness is shown as Figure S7 in the SI.

Lithium−Oxygen Battery Assembly. Lithium−oxygen batteries were assembled in an argon-filled glovebox with oxygen and water contents less than 1 ppm. The batteries have a coin-cell structure consisting of a stainless steel anode shell, a metallic lithium foil anode (0.5 mm thick), a Celgard 3501 separator (from Celgard LLC), as-synthesized carbon cathode (CF or graphene sponge), a nickel foam current collector and a stainless steel cathode shell with holes in it. The lithium foil was treated with 0.1 mol l^{-1} $LiClO_4$−propylene carbonate (PC) solution for at least 3 days before usage to form an SEI layer to protect the anode. A homemade device may be added to depress the DMSO evaporation (Figure S6 in the SI). The cathode loading density was about 1 mg cm^{-2} for CFs or 0.25 mg cm^{-2} for graphene sponges. The amount of the electrolyte was 8 μL.

Electrochemical Performance Test. The galvanostatic discharge and charge tests were conducted on a LAND CT2001A battery system.

XRD, SEM, EDX, XPS Characterizations. The discharge and charge products were washed with pure DMSO before characterization. The XRD test was conducted with a rotating copper Kα radiation (PANalytical B.V., Holland). EDX and SEM data were obtained with a SIRION200 SEM machine. The XPS experiment was performed on an ESCALAB 250Xi XPS system with a monochromatic Al X-ray source (1486.6 eV).

ICP-AES Analysis. The amount of Fe element adsorbed on the Li anode after 10 cycles of discharge/charge at 1000 mA h g^{-1} was measured with ICP-AES (Perkin Elmer, Optima4300DV). The whole anode was put into water to make the solution for measurement.

ASSOCIATED CONTENT

Supporting Information

Calculation details, proofs of the Li_2O_2 blocking effect, characterization of Fe−N/C CFs, experimental set-ups. This material is available free of charge via the Internet at http://pubs.acs.org.

AUTHOR INFORMATION

Corresponding Authors

shenyue1213@hust.edu.cn (Y.S.)
huangyh@mail.hust.edu.cn (Y.H.)

Notes

The authors declare no competing financial interest.

ACKNOWLEDGMENTS

The authors thank Analytical and Testing Center of HUST for XRD and SEM measurements. This work is supported by the Natural Science Foundation of China (51202076, 50825203, 20825520), China Postdoctoral Science Foundation (2012M510178, 2013T60716), Ministry of Science and Technology of China (2011YQ12003503), and the Robet A. Welch Foundation Grant Number F-1066, Houston, Texas.

REFERENCES

(1) Abraham, K. M.; Jiang, Z. *J. Electrochem. Soc.* **1996**, *143*, 1.

(2) Bruce, P. G.; Freunberger, S. A.; Hardwick, L. J.; Tarascon, J.-M. *Nat. Mater.* **2012**, *11*, 19.
(3) Zhang, T.; Imanishi, N.; Takeda, Y.; Yamamoto, O. *Chem. Lett.* **2011**, *40*, 668.
(4) Lu, Y.-C.; Gallant, B. M.; Kwabi, D. G.; Harding, J. R.; Mitchell, R. R.; Whittingham, M. S.; Shao-Horn, Y. *Energy Environ. Sci.* **2013**, *6*, 750.
(5) Cheng, F.; Chen, J. *Chem. Soc. Rev.* **2012**, *41*, 2172.
(6) Shao, Y.; Park, S.; Xiao, J.; Zhang, J.-G.; Wang, Y.; Liu, J. *ACS Catal.* **2012**, *2*, 844.
(7) Thapa, A. K.; Saimen, K.; Ishihara, T. *Electrochem. Solid-State Lett.* **2010**, *13*, A165.
(8) Lu, Y.-C.; Xu, Z.; Gasteiger, H. A.; Chen, S.; Hamad-Schifferli, K.; Shao-Horn, Y. *J. Am. Chem. Soc.* **2010**, *132*, 12170.
(9) Benbow, E. M.; Kelly, S. P.; Zhao, L.; Reutenauer, J. W.; Suib, S. L. *J. Phys. Chem. C* **2011**, *115*, 22009.
(10) Wang, L.; Zhao, X.; Lu, Y.; Xu, M.; Zhang, D.; Ruoff, R. S.; Stevenson, K. J.; Goodenough, J. B. *J. Electrochem. Soc.* **2011**, *158*, A1379.
(11) Li, J.; Wang, N.; Zhao, Y.; Ding, Y.; Guan, L. *Electrochem. Commun.* **2011**, *13*, 698.
(12) Lim, H.-D.; Gwon, H.; Kim, H.; Kim, S.-W.; Yoon, T.; Choi, J. W.; Oh, S. M.; Kang, K. *Electrochim. Acta* **2013**, *90*, 63.
(13) Yoon, T. H.; Park, Y. J. *Nanoscale Res. Lett.* **2012**, *7*, 28.
(14) Cui, Y.; Wen, Z.; Liu, Y. *Energy Environ. Sci.* **2011**, *4*, 4727.
(15) Zhang, S. S.; Ren, X.; Read, J. *Electrochim. Acta* **2011**, *56*, 4544.
(16) Wu, J.; Park, H. W.; Yu, A.; Higgins, D.; Chen, Z. *J. Phys. Chem. C* **2012**, *116*, 9427.
(17) Shui, J.-L.; Karan, N. K.; Balasubramanian, M.; Li, S.-Y.; Liu, D.-J. *J. Am. Chem. Soc.* **2012**, *134*, 16654.
(18) Zhang, T.; Zhou, H. *Angew. Chem., Int. Ed.* **2012**, *51*, 11062.
(19) Kitaura, H.; Zhou, H. *Adv. Energy Mater.* **2012**, *2*, 889.
(20) Mitchell, R. R.; Gallant, B. M.; Thompson, C. V.; Shao-Horn, Y. *Energy Environ. Sci.* **2011**, *4*, 2952.
(21) Zhang, T.; Zhou, H. *Nat. Commun.* **2013**, *4*, 1817.
(22) Wang, Z.-L.; Xu, D.; Xu, J.-J.; Zhang, L.-L.; Zhang, X.-B. *Adv. Funct. Mater.* **2012**, *22*, 3699.
(23) Sun, B.; Wang, B.; Su, D.; Xiao, L.; Ahn, H.; Wang, G. *Carbon* **2012**, *50*, 727.
(24) Yoo, E.; Nakamura, J.; Zhou, H. *Energy Environ. Sci.* **2012**, *5*, 6928.
(25) Xiao, J.; Mei, D.; Li, X.; Xu, W.; Wang, D.; Graff, G. L.; Bennett, W. D.; Nie, Z.; Saraf, L. V.; Aksay, I. A.; Liu, J.; Zhang, J.-G. *Nano Lett.* **2011**, *11*, 5071.
(26) Xu, J.-J.; Xu, D.; Wang, Z.-L.; Wang, H.-G.; Zhang, L.-L.; Zhang, X.-B. *Angew. Chem., Int. Ed.* **2013**, *52*, 3887.
(27) Zhao, Y.; Xu, L.; Mai, L.; Han, C.; An, Q.; Xu, X.; Liu, X.; Zhang, Q. *Proc. Natl. Acad. Sci. U.S.A.* **2012**, *109*, 19569.
(28) Oh, S. H.; Black, R.; Pomerantseva, E.; Lee, J.-H.; Nazar, L. F. *Nat. Chem.* **2012**, *4*, 1004.
(29) Shao, Y.; Ding, F.; Xiao, J.; Zhang, J.; Xu, W.; Park, S.; Zhang, J.-G.; Wang, Y.; Liu, J. *Adv. Funct. Mater.* **2013**, *23*, 987.
(30) Trahan, M. J.; Mukerjee, S.; Plichta, E. J.; Hendrickson, M. A.; Abraham, K. M. *J. Electrochem. Soc.* **2013**, *160*, A259.
(31) McCloskey, B. D.; Scheffler, R.; Speidel, A.; Bethune, D. S.; Shelby, R. M.; Luntz, A. C. *J. Am. Chem. Soc.* **2011**, *133*, 18038.
(32) Chen, Y.; Freunberger, S. A.; Peng, Z.; Fontaine, O.; Bruce, P. G. *Nat. Chem.* **2013**, *5*, 489.
(33) Lim, H.-D.; Song, H.; Kim, J.; Gwon, H.; Bae, Y.; Park, K.-Y.; Hong, J.; Kim, H.; Kim, T.; Kim, Y. H.; Lepró, X.; Ovalle-Robles, R.; Baughman, R. H.; Kang, K. *Angew. Chem., Int. Ed.* **2014**, *53*, 3926.
(34) Chase, G. V.; Zecevic, S.; Walker, W.; Uddin, J.; Sasaki, K. A.; Giordani, V.; Bryantsev, V.; Blanco, M.; Addison, D. D. Soluble oxygen evolving catalysts for rechargeable metal-air batteries. Patent WO2011133982A1, 2011.
(35) Jahnke, H.; Schonborn, M.; Zimmermann, G. *Top. Curr. Chem.* **1976**, *61*, 133.
(36) Bezerra, C. W. B.; Zhang, L.; Lee, K.; Liu, H.; Marques, A. L. B.; Marques, E. P.; Wang, H.; Zhang, J. *Electrochim. Acta* **2008**, *53*, 4937.
(37) He, Q.; Mugadza, T.; Kang, X.; Zhu, X.; Chen, S.; Kerr, J.; Nyokong, T. *J. Power Sources* **2012**, *216*, 67.
(38) Cao, R.; Thapa, R.; Kim, H.; Xu, X.; Gyu Kim, M.; Li, Q.; Park, N.; Liu, M.; Cho, J. *Nat. Commun.* **2013**, *4*, 2076.
(39) Peng, Z.; Freunberger, S. A.; Chen, Y.; Bruce, P. G. *Science* **2012**, *337*, 563.
(40) Laoire, C.; Mukerjee, S.; Plichta, E. J.; Hendrickson, M. A.; Abraham, K. M. *J. Electrochem. Soc.* **2011**, *158*, A302.
(41) Jung, H.-G.; Hassoun, J.; Park, J.-B.; Sun, Y.-K.; Scrosati, B. *Nat. Chem.* **2012**, *4*, 579.
(42) C.Leznoff, C.; B, L. A. In *Phthalocyanine Properties and Applications*; VCH Publishers, Inc: New York, 1989; p 397.
(43) Lever, A. B. P.; Wilshire, J. P. *Inorg. Chem.* **1978**, *17*, 1145.
(44) Yin, G. *Coord. Chem. Rev.* **2010**, *254*, 1826.
(45) Zussman, E.; Yarin, A. L.; Bazilevsky, A. V.; Avrahami, R.; Feldman, M. *Adv. Mater.* **2006**, *18*, 348.
(46) Sun, H.; Xu, Z.; Gao, C. *Adv. Mater.* **2013**, *25*, 2554.
(47) Lacey, M. J.; Frith, J. T.; Owen, J. R. *Electrochem. Commun.* **2013**, *26*, 74.
(48) Younesi, R.; Hahlin, M.; Roberts, M.; Edström, K. *J. Power Sources* **2013**, *225*, 40.
(49) Shui, J.-L.; Okasinski, J. S.; Kenesei, P.; Dobbs, H. A.; Zhao, D.; Almer, J. D.; Liu, D.-J. *Nat. Commun.* **2013**, *4*, 2255.
(50) Knauth, P. *Solid State Ionics* **2009**, *180*, 911.
(51) Xu, Z.; Sun, H.; Zhao, X.; Gao, C. *Adv. Mater.* **2013**, *25*, 188.

NOTE ADDED AFTER ASAP PUBLICATION

After the ASAP version of this article was posted June 12, 2014, patent citation ref 34 was added, and all subsequent reference numbers were incremented accordingly. The corrected version was reposted June 17, 2014.